Yielding of glass under shear: A directed percolation transition precedes shear-band formation

Gaurav Prakash Shrivastav,[1] Pinaki Chaudhuri,[2] and Jürgen Horbach[1]
[1]*Institut für Theoretische Physik II, Heinrich-Heine-Universität Düsseldorf, Universitätsstraße 1, 40225 Düsseldorf, Germany*
[2]*The Institute of Mathematical Sciences, CIT Campus, Taramani, Chennai 600 113, India*
(Received 24 January 2016; published 19 October 2016)

Under external mechanical loading, glassy materials, ranging from soft matter systems to metallic alloys, often respond via formation of inhomogeneous flow patterns, during yielding. These inhomogeneities can be precursors to catastrophic failure, implying that a better understanding of their underlying mechanisms could lead to the design of smarter materials. Here, extensive molecular dynamics simulations are used to reveal the emergence of heterogeneous dynamics in a binary Lennard-Jones glass, subjected to a constant strain rate. At a critical strain, this system exhibits for all considered strain rates a transition towards the formation of a percolating cluster of mobile regions. We give evidence that this transition belongs to the universality class of directed percolation. Only at low shear rates, the percolating cluster subsequently evolves into a transient (but long-lived) shear band with a diffusive growth of its width. Finally, the steady state with a homogeneous flow pattern is reached. In the steady state, percolation transitions also do occur constantly, albeit over smaller strain intervals, to maintain the stationary plastic flow in the system.

DOI: 10.1103/PhysRevE.94.042605

I. INTRODUCTION

An external shear field leads in general to a rejuvenation of the glass state, transforming the amorphous solid into a flowing fluid [1,2]. Under a constant strain rate, the transition to plastic flow can be located via the dependence of the shear stress on the applied strain. It is marked by a maximum in the stress-strain relation, the stress overshoot, which for a simple planar Couette flow geometry occurs typically at a strain of the order of 0.1 [2–5]. Beyond this maximum, the system evolves into a steady-state regime where it displays a homogeneous flow pattern, e.g., in the case of planar Couette flow, manifested as a linear velocity profile. However, the strain necessary to reach this steady-state regime depends on many factors such as the history of the initial undeformed glass state and the applied strain rate [6,7].

In the transient regime before the steady state is reached, the emergence of spatially inhomogeneous flow patterns is very common. These are initiated by localized plastic events that appear prior to the occurrence of the stress overshoot [2,8]. Subsequently, an inhomogeneous response in the form of shear bands [9–14], with co-existing regions of contrasting mobilities spanning large scales [9], is often observed. Despite the fact that dynamical heterogeneities, in various forms, be it during yielding or during steady flow, have been detected in experiments [15–18], numerical simulations [19–28], and phenomenological models [29–32], the microscopic processes that eventually lead to the formation of such complex structures, whether transient or persistent, still remain ill understood.

The question about the origin of the inhomogeneous response is intimately related to the question of how flow is initiated in an amorphous solid under applied shear. Recent studies suggest that the response of the glass to the applied strain is governed by local heterogeneities that are either already present in the undeformed solid or form during the initial application of the shear field [1,2,4]. These heterogeneities are associated with "hot spots" of higher mobility that grow while the strain of the system increases [33,34].

In this work, we focus both on the onset of plastic flow and the formation of flow heterogeneities in thermal glasses, which are often characterized as simple yield stress fluids [35]. In such a system, we first reveal the nature of the yielding transition under applied shear. Subsequently, we demonstrate how shear bands emerge and evolve, once the glass has yielded. Note that our analysis is probably only generic to simple thermal glasses (e.g., in the context of soft matter systems, colloids, emulsions, etc.) and not to other solids such as gels [36–39] or network-forming glasses such as silica [40,41].

In the case of thermal systems yielding under a finite applied shear rate, the interplay of thermal noise and external mechanical load leads to local structural rearrangements. As a consequence, the yielding process is more complex than for athermal systems, and thus different from the quasistatic limit where many of the investigations have been focused so far. In our studies of a sheared thermal model glass under constant strain rate, we identify the hot spots using local mean-squared displacements (MSDs) and explore their spatiotemporal evolution using MSD maps [20,34]. The hot spots develop into clusters of mobile regions, associated with a correlation length that grows with increasing strain and that eventually diverges at a critical strain where the mobile regions exhibit a percolation transition. This transition marks the transformation of the system from a nonflowing state to plastic flow. We give evidence that it belongs to the universality class of directed percolation (DP), as expected for systems under external drives. Different from normal percolation, DP is associated with an anisotropic growth of the correlation length towards the critical point. As put forward by the DP conjecture [42,43], DP universality is believed to be very robust, applying to a broad class of nonequilibrium phase transitions [44]. However, up to now there are only a few examples where DP transitions have been found in experimental systems (see, e.g., Refs. [45,46]). Here, we demonstrate that a DP transition marks the onset of flow in a sheared glass and is the basis for the possible formation and growth of shear bands.

We use large-scale molecular dynamics (MD) simulations of a binary Lennard-Jones (LJ) mixture [47] to study the mechanical response of a quiescent amorphous solid when an external shear rate is imposed on it. We track the locations of

regions of large mobilities and thereby we reveal the existence of the DP transition driven in the direction of applied shear. While the DP transition is seen for all shear rates, visible shear banding only emerges for small shear rates near the yielding threshold. We demonstrate that the glass eventually fluidizes by the long-time diffusive invasion of the shear band into the rest of the system, with the diffusion time scales dependent on the imposed shear rates. Thus, we provide a quantitative description of how initial local mobilities build up to the eventual macroscopic flow of the material. In the steady state, percolation transitions constantly occur in small strain intervals, $\Delta\gamma_c \approx 0.02$. These transitions keep the system in a flowing state.

II. METHODS

Our focus is on the understanding of the yielding response of a quiescent thermal glass. We consider a well-studied glass forming system: a binary 80:20 mixture of LJ particles (say A and B). The interaction between a pair of particles, separated by a distance r, is defined as

$$U^{\mathrm{LJ}}_{\alpha\beta}(r) = \phi_{\alpha\beta}(r) - \phi_{\alpha\beta}(R_c) - (r - R_c)\left.\frac{d\phi_{\alpha\beta}}{dr}\right|_{r=R_c},$$
$$\phi_{\alpha\beta}(r) = 4\epsilon_{\alpha\beta}[(\sigma_{\alpha\beta}/r)^{12} - (\sigma_{\alpha\beta}/r)^{6}], \quad (1)$$

for $r < R_c$, with $\alpha,\beta = \mathrm{A}, \mathrm{B}$. The parameters setting the energy scale are defined as $\epsilon_{\mathrm{AA}} = 1.0$, $\epsilon_{\mathrm{AB}} = 1.5\epsilon_{\mathrm{AA}}$, $\epsilon_{\mathrm{BB}} = 0.5\epsilon_{\mathrm{AA}}$. The parameters with the unit of a length are given as $\sigma_{\mathrm{AA}} = 1.0$, $\sigma_{\mathrm{AB}} = 0.8\sigma_{\mathrm{AA}}$, $\sigma_{\mathrm{BB}} = 0.88\sigma_{\mathrm{AA}}$ and the range of the interactions is set to $R_c = 2.5\sigma_{\mathrm{AA}}$. Thus, energies and lengths are expressed in units of ϵ_{AA} and σ_{AA}, respectively. The masses of both types of particles are equal, i.e., $m_{\mathrm{A}} = m_{\mathrm{B}} = m$. The unit of time is $\sqrt{m\sigma^2_{\mathrm{AA}}/\epsilon_{\mathrm{AA}}}$. In the following, all the quantities are expressed in the latter units. More details on the model and the interaction parameters can be found in Ref. [47]. We note, here, that a wide variety of dense soft glasses, like colloids, emulsions, etc., can be modeled by using such LJ mixtures.

Using the package LAMMPS ("Large-scale Atomic/Molecular Massively Parallel Simulator") [48], we perform MD simulation at constant particle number, N, constant volume, V, and constant temperature, T (i.e., in the NVT ensemble). Different geometries are considered, placing the particles in boxes of dimensions $10 \times 10 \times 40$, $15 \times 15 \times 60$, $20 \times 20 \times 80$, $25 \times 25 \times 100$, $30 \times 30 \times 120$, $40 \times 40 \times 40$, and $50 \times 50 \times 50$. The temperature is kept constant via a dissipative particle dynamics (DPD) thermostat [49].

Our method for the preparation of glass is as follows: At a density $\rho = 1.2$, we first equilibrate the system at the temperature $T = 0.45$, which is in the supercooled regime. Then, we quench it to a temperature $T = 0.2$ below the mode coupling transition temperature [47]. We wait until $t_{\mathrm{w}} = 10^4$ and apply shear on the xz plane in the direction of x with different constant strain rates $\dot{\gamma} = 10^{-2}, 10^{-3}, 3 \times 10^{-4}, 10^{-4}, 3 \times 10^{-5}$, and 10^{-5}. To simulate a sheared bulk glass, we use Lees-Edwards periodic boundary conditions [50].

We also do simulations for a denser glass ($\rho = 1.3$), where we first equilibrate a supercooled system at the temperature $T = 0.67$. Then, it is quenched to $T = 0.10$, far below the mode coupling transition temperature, and aged for $t_{\mathrm{w}} = 10^4$. We choose a long aging time, since we are interested in probing the formation of dynamical heterogeneities which are expected to be observed for large t_{w}.

III. RESULTS

A. How to identify hot spots

When the shear is applied to the quiescent glass at time $t = 0$, the material deforms exhibiting the typical stress (σ) versus strain ($\dot{\gamma}t$) response [shown in Fig. 1(a) for different imposed shear rates $\dot{\gamma}$], with the height of the overshoot depending on $\dot{\gamma}$ [6]. The measured steady-state stress as a function of the imposed shear rate is shown in the inset of Fig. 1(a); it has the typical Herschel-Bulkley form [6]. The monotonic shape of the flow curve implies that there are no mechanical instabilities. Thus, in this system, there are no permanent flow heterogeneities, which are known to exist when steady-state flow curves are nonmonotonic [13,14,28,31]. We note that monotonic flow curves such as the one shown in Fig. 1(a) are typical to most dense soft glasses [17,51].

During the onset of flow from the quiescent state, the corresponding single particle dynamics can be quantified by measuring the nonaffine MSD, $\Delta {r_z}^2$, in the direction transverse to the applied shear; the data are shown in Fig. 1(b). The particles undergo ballistic motion at early times and are then caged, before the occurrence of a superdiffusive regime, prior to diffusion. The onset of superdiffusion occurs around the stress overshoot in the stress-strain curve, when the built-up stress is released via the particles breaking their local cages to subsequently diffuse [3].

In experiments, flow heterogeneities are often diagnosed via the spatial profiles of local velocities [15,17]. Similarly, we measure the spatial profiles of the local flow velocities (averaged over strain intervals of 0.5%), $v_x(z)$, for an imposed shear rate of 10^{-4}, at different times after the imposition of shear [marked on the corresponding stress-strain curve in Fig. 1(a)]. The spatial profiles are shown in Fig. 1(c) for one of the initial states in our ensemble. In the elastic regime, at $\dot{\gamma}t = 0.02$, the velocity profile is linear, but starts deviating from this shape as the stress overshoot is approached at $\dot{\gamma}t = 0.06$. This deviation becomes stronger in the transient regime (at $\dot{\gamma}t = 0.5$, shown in blue diamonds). Interestingly, the velocity profile regains its linear shape as plastic flow sets in (at $\dot{\gamma}t = 1.0$, shown in orange stars). The observation of increased heterogeneity, after the stress overshoot, is consistent with experimental observations [15].

However, local velocity profiles only capture the short-time heterogeneities in dynamics. In order to obtain a more cumulative picture from $t = 0$, we look at the spatially resolved maps of $\Delta {r_z}^2(t)$ [20,52]. To construct the MSD maps, we divide the simulation box into small cubic sub-boxes having linear size of σ_{AA}. At any time t, we calculate the average MSD of the particles populating each sub-box at $t = 0$ (unsheared glassy state). In Fig. 1(d), we show the time evolution of such a map, for an initial state under the imposed shear rate of

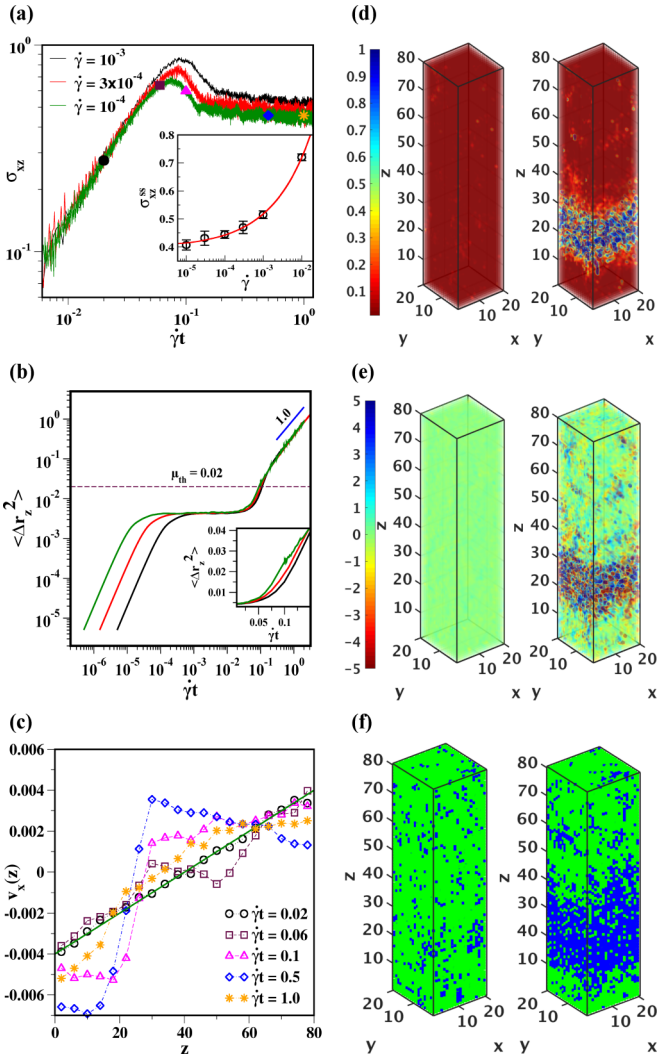

FIG. 1. (a) Stress-strain response of the glass at temperature $T = 0.2$ for an age of $t_w = 10^4$ and sheared with a constant strain rate. Data shown for different shear rates: $\dot{\gamma} = 10^{-3}$,3×10^{-4}, and 10^{-4}. The inset shows the flow curve. Red solid line shows the fitting with Herschel-Bulkley form $\sigma_{xz}^{ss}(\dot{\gamma}) = 0.3974 + 2.2963\dot{\gamma}^{0.43}$. (b) Variation of z component of the MSD of large particles with strain. Brown dotted line marks μ_{th}. The inset is a zoom into the superdiffusive regime for the three different shear rates, shown in linear scale. (c) Velocity profiles, for $\dot{\gamma} = 10^{-4}$, at five different strain values marked in (a). Green solid line represents the expected linear profile. (d) MSD maps at $\dot{\gamma}t = 0.06$,0.5 for $\dot{\gamma} = 10^{-4}$. (e) Maps of local strain corresponding to MSD maps shown in (d). (f) Maps of local mobility corresponding to (d). Mobile regions are marked in blue while immobile regions are marked in green.

$\dot{\gamma} = 10^{-4}$. At a strain of $\dot{\gamma}t = 0.06$, the local dynamics is nearly homogeneous on this scale. However, at $\dot{\gamma}t = 0.5$, spatially heterogeneous dynamics is observed, with the more mobile particles localized in a shear-band-like structure spanning the xy plane.

We can also construct similar maps of local strain. Again, we divide the simulation box into small cubic sub-boxes, as in the case of MSD maps. The numerical derivative of the z component of displacement with respect to x, i.e., $\epsilon_{zx} = \partial \Delta r_z / \partial x$, is calculated. This derivative is plotted for each sub-box to construct the map. These maps exhibit a localization behavior similar to the MSD maps; see Fig. 1(e). Thus, large local MSDs are also regions of large strains. Henceforth, we use $\Delta {r_z}^2$ to analyze local dynamical properties.

B. Yielding: A percolation transition

In order to quantify and characterize the spatiotemporal evolution of the mobile regions, we define a region to be mobile or not, by setting a threshold $\mu_{th} = 0.02$ on the local $\Delta {r_z}^2$. As marked by the dashed line in Fig. 1(c), such a choice of μ_{th} is larger than the plateau value in the MSD and thus corresponds to motions beyond cage breaking. We then define the local mobility ψ as

$$\psi = \begin{cases} 1 & \text{if } \mu \geqslant \mu_{th} \\ 0 & \text{otherwise} \end{cases}, \tag{2}$$

where μ is the average MSD of particles in a sub-box. Following this convention, we digitize the whole system into mobile and immobile regions. The mobility maps corresponding to Fig. 1(d) are shown in Fig. 1(f). We also note that there is a slight dependence of results on the choice of threshold but the qualitative behavior does not change.

We now demonstrate that a percolation transition occurs with increasing strain, involving these mobile regions. As the system evolves under the applied shear rate, we monitor the fraction of mobile cells, p, at any given instant. Figure 1(d) suggests that such mobile regions do form clusters. Thus, we compute what fraction of these mobile regions, p_{span}, is part of a cluster that spans the system, recalling that such an observable is the order parameter for determining the occurrence of a percolation transition. In Fig. 2(a), we plot p_{span} as a function of p, which shows that beyond a critical fraction p_c all the mobile cells are part of such a spanning cluster. This indicates the occurrence of a percolation transition of these mobile cells. Furthermore, we observe that the variation of p_c is nearly independent of the imposed shear rate, as seen in Fig. 2(a) for a wide range of $\dot{\gamma}$. Thus, the percolation process is generic to the system's response under shear. In Fig. 2(b), we visualize the spanning clusters corresponding to the same initial state, for three different shear rates, in the vicinity of p_c corresponding to each $\dot{\gamma}$. Here, we note that the near localization of the spanning cluster in the xy plane is a finite-size effect, due to the large aspect ratio of the simulation box. This is clarified when we visualize the spanning cluster in a cubic geometry, as shown in Fig. 2(c) for $\dot{\gamma} = 10^{-4}$ in a 50^3 system, which is indeed a three-dimensional fractal object.

Next, for different imposed $\dot{\gamma}$, if we monitor the numerical growth of mobile cells with increasing strain, a distinct variation is revealed; see Fig. 2(d). For example, at a strain of $\dot{\gamma}t = 0.5$ (marked by orange dotted line), we see that around 50% of the sites are mobile at low strain rates while the same is close to 75% at high strain rates. This implies that subsequent to the percolation transition (at the critical strain corresponding to p_c, which is around 0.07 for $\dot{\gamma} = 10^{-4}$) the spatial heterogeneity of activity is more long lived for smaller strain rates, as is shown in Fig. 2(c), via cuts in the xz plane of the local MSD maps corresponding to the evolving trajectories of the states shown in Fig. 2(b). While for the

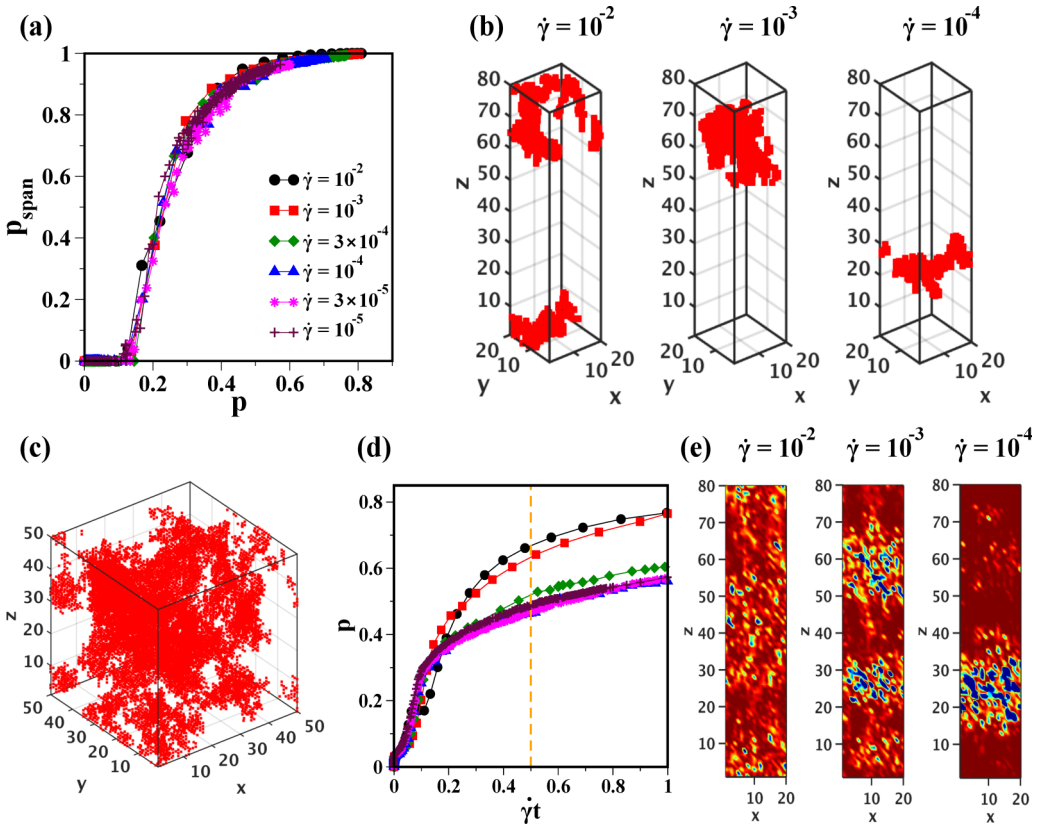

FIG. 2. Emergence of percolation transition. (a) Variation of p_{span} with p, in the box of dimension $20 \times 20 \times 80$, for strain rates $\dot\gamma = 10^{-2}, 10^{-3}, 3 \times 10^{-4}, 10^{-4}, 3 \times 10^{-5}$, and 10^{-5}. (b) Percolating cluster at the critical point for $\dot\gamma = 10^{-2}, 10^{-3}$, and 10^{-4} (left to right) in a $20 \times 20 \times 80$ system. (c) Percolating cluster at the critical point for $\dot\gamma = 10^{-4}$ in a 50^3 system. (d) Variation of p with strain for all strain rates shown in (a). Orange dotted line corresponds to the $\dot\gamma t = 0.5$. (e) 2D slice of MSD map for trajectories shown in (b), at $\dot\gamma t = 0.5$.

largest shear rate mobile regions proliferate in the system, for the smaller shear rate they are more localized and take the form of a well-structured shear band. Thus, one can infer that the local dynamics, post-percolation, changes with decreasing shear rate.

To clarify the nature of the percolation transition, we determine the critical point for the percolation process, p_c, using finite-size scaling. In Fig. 3(a), we show how p_{span} varies with p for five different system sizes—we observe that the onset of percolation shifts to larger values of p with

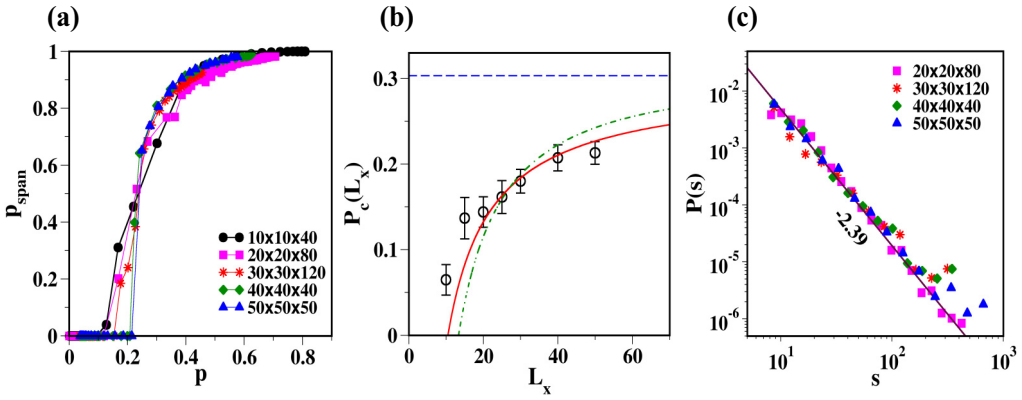

FIG. 3. Occurrence of directed percolation (DP) transition. (a) Variation of p_{span} with p for five different system sizes $10 \times 10 \times 40$ (black circles), $20 \times 20 \times 80$ (magenta squares), $30 \times 30 \times 120$ (red stars), $40 \times 40 \times 40$ (green diamonds), $50 \times 50 \times 50$ (blue triangles) for $\dot\gamma = 10^{-4}$. (b) Finite-size scaling of critical points for the systems sizes shown in (a); the red solid line shows the fit according to the scaling law $p_c(L_x) = 0.3034 - 2.412 L_x^{-1/1.106}$ corresponding to DP. Green dash-dotted line shows the same scaling function with parameters corresponding to standard percolation: critical point $p_c(\infty) = 3.116$ and $\nu = 0.8765$. The blue dotted line shows the asymptotic $p_c(\infty)$ for DP which is 0.3034. (c) Cluster size distribution around p_c for the system sizes shown in (a); data show a power-law decay with exponent -2.39 which is consistent with the prediction for DP.

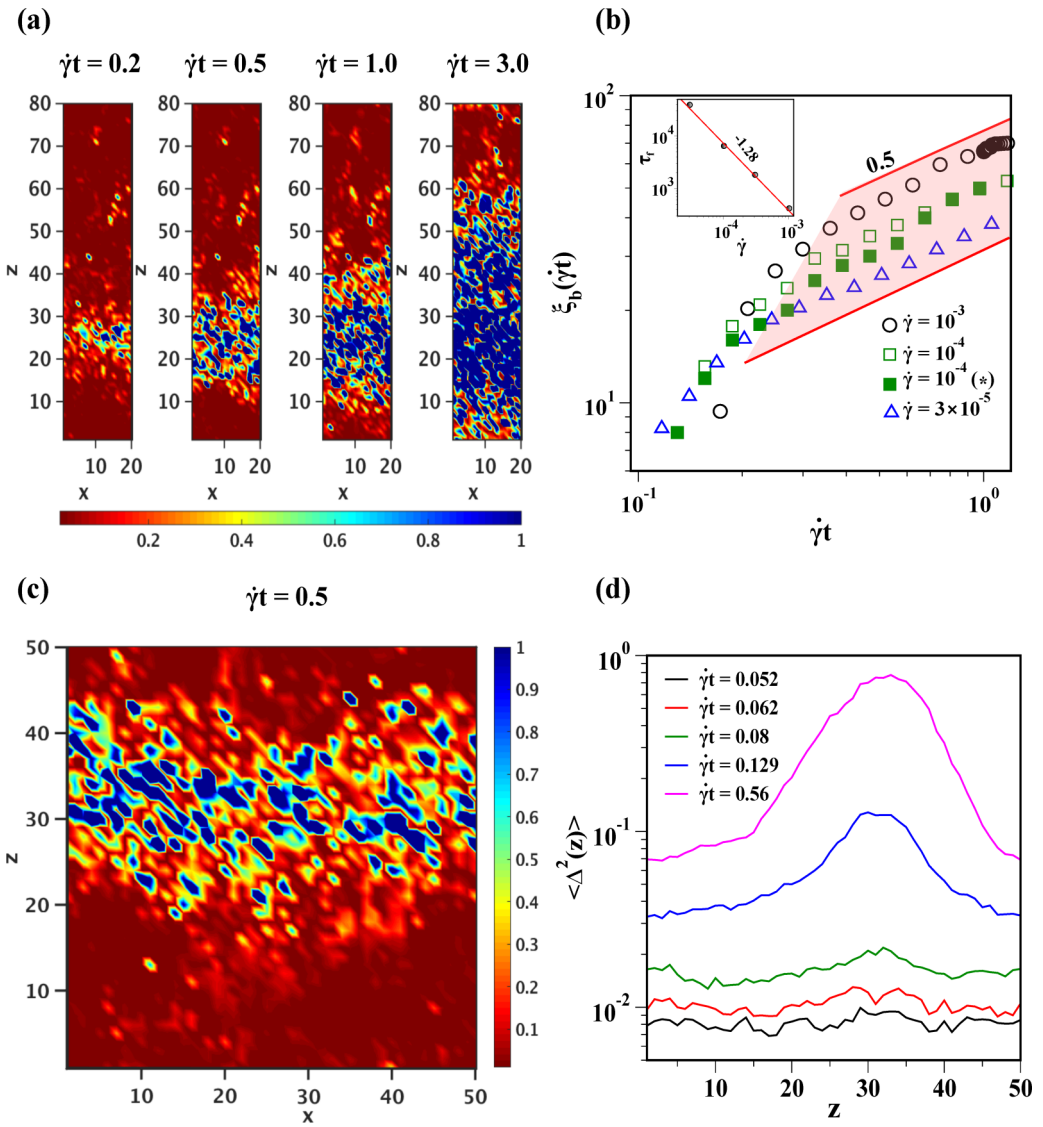

FIG. 4. (a) 2D projections, in xz plane, of MSD maps for $20 \times 20 \times 80$ showing the evolution of shear band with time, for imposed $\dot{\gamma} = 10^{-4}$, at strains of $\dot{\gamma}t = 0.2, 0.5, 1.0, 3.0$. (b) Variation of width of the band ξ_b, with $\dot{\gamma} = 10^{-3}, 10^{-4}, 3 \times 10^{-5}$. Also shown, using solid green squares, is the growth of ξ_b in a 50^3 system, for $\dot{\gamma} = 10^{-4}$. The zone between the solid red lines marks the regime of $t^{1/2}$ growth. Inset shows the dependence of time scale for fluidization, τ_f (defined in the text), with changing $\dot{\gamma}$; the red line is a fit with $\dot{\gamma}^{-1.28}$. (c) 2D projection of MSD map for a 50^3 system at $\dot{\gamma}t = 0.5$ sheared with $\dot{\gamma} = 10^{-4}$. (d) Corresponding evolution of spatial profile of mobility, $\Delta^2(z)$, with strain, in the 50^3 system.

increasing system size. In Fig. 3(b), we show that the threshold obtained for different system sizes can be well described by the finite-size scaling function $p_c(L_x) = p_c(\infty) + bL_x^{-1/\nu_\parallel}$ [53], using $p_c(\infty) = 0.3034$ and $\nu_\parallel = 1.106$, which are values corresponding to a DP transition [54], with L_x being the length of the box in the direction of the applied shear. To compare, the corresponding numbers for standard percolation are $p_c(\infty)$ $(= 0.3116)$ and ν $(= 0.8765)$ [55]; the finite-size scaling function using these parameters does not at all describe our data [see Fig. 3(b), green line]. Furthermore, we compute the size distribution of clusters of mobile cells in the vicinity of the percolation transition [Fig. 3(c)]. As expected, the distribution has a power-law shape, with the corresponding DP exponent of -2.39 well characterizing the distribution [55,56]. Thus, the percolation of the active regions, in this regime of flow, is a directed process, driven in the direction of the external shear.

C. Post-percolation: Formation and growth of shear bands

Thus far, we have discussed the existence of an underlying percolation process of the mobile regions, which occurs for the entire range of $\dot{\gamma}$ that we have studied. Now, we will focus on how the dynamics proceeds once the percolating cluster has formed. In order to quantify that, we construct MSD maps (now with a threshold $\mu_{\rm th} = 0.1$). In Fig. 4(a), we show the time evolution of the local mobility, via two-dimensional (2D) projection of such maps, for $\dot{\gamma} = 10^{-4}$. We observe that the z width of the shear band increases with time and eventually the

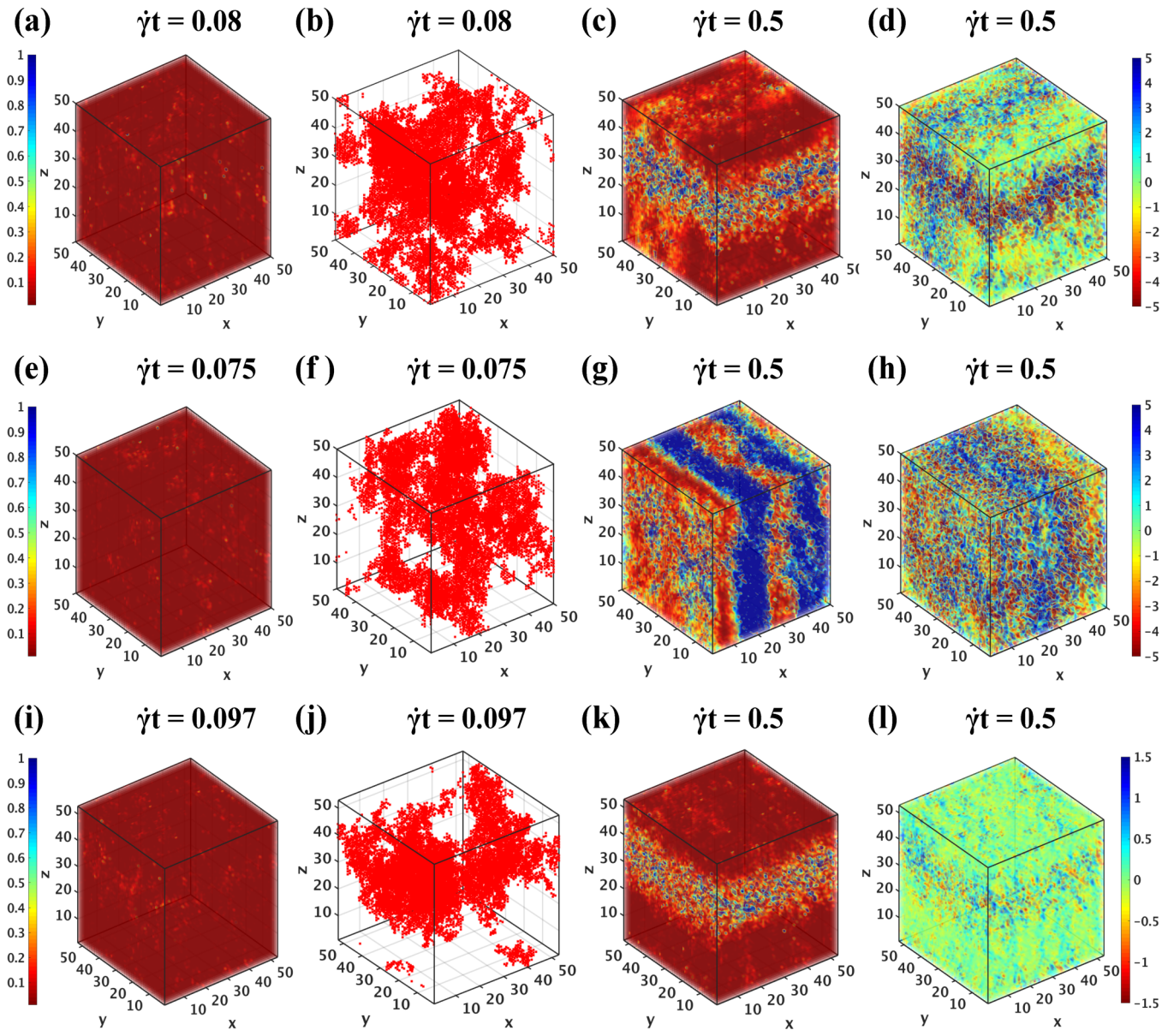

FIG. 5. Evolution of flow patterns in different samples. The upper and middle panel show data for 50^3 system at density 1.2 and temperature $T = 0.2$. Lower panel shows the similar data for 53^3 system at density 1.3 and temperature $T = 0.1$. All the three samples are sheared with constant strain rate $\dot{\gamma} = 10^{-4}$. (a), (e), and (i) show MSD map around percolation transition, (b), (f), and (j) show percolating cluster near the transition point. (c), (g), and (k) show MSD map at large strain while (d), (h), and (l) show strain map at the same strain.

entire system becomes mobilized. To quantitatively identify a shear band, we divide the simulation box into xy layers with a thickness of one particle diameter and calculate μ, which is the z component of MSD, for each layer. We assign to each layer a value $\psi = 1$ or 0 depending on whether μ is larger or smaller than $\mu_{\rm th}$. To get the size of the shear band, we count the number of adjoining layers for which $\psi = 1$. By marking the interfaces of this band, we measure how the bandwidth, $\xi_{\rm b}$, evolves with time. For different imposed shear rates, this time evolution is shown in Fig. 4(b). We see that $\xi_{\rm b}$ initially grows quickly and then eventually it reaches a regime where the data can be fitted with $\xi_{\rm b} \sim t^{1/2}$, implying that the propagating interface of the shear band has a diffusive motion. The diffusion constant is dependent on the imposed shear rate. The smaller the shear rate $\dot{\gamma}$, the slower is the diffusion, which leads to more long-lived heterogeneities, as discussed earlier. For the largest shear rate shown, $\dot{\gamma} = 10^{-3}$, the diffusive regime is very short lived as the band quickly spans the entire system. For even larger shear rates, beyond percolation, mobile regions quickly appear everywhere and fluidize the whole system, and, as a consequence, a shear band is not clearly discernible. Further, from the data for the growth of $\xi_{\rm b}$, we extract the characteristic time scale for the system to fluidize, τ_f, viz., $\xi_{\rm b}(\tau_f) = 40\sigma_{\rm AA}$, for different imposed shear rates; see inset in Fig. 4(b). We see that $\tau_f \sim \dot{\gamma}^{-1.28}$; such a diverging time scale for fluidization, in the vicinity of the yield stress, is consistent with earlier measurements in simple yield stress fluids [15,20,57].

Here, we emphasise that the occurrence of a shear band is not a finite-size effect. Similar spatial localization of dynamics is also observed in cubic systems, as depicted

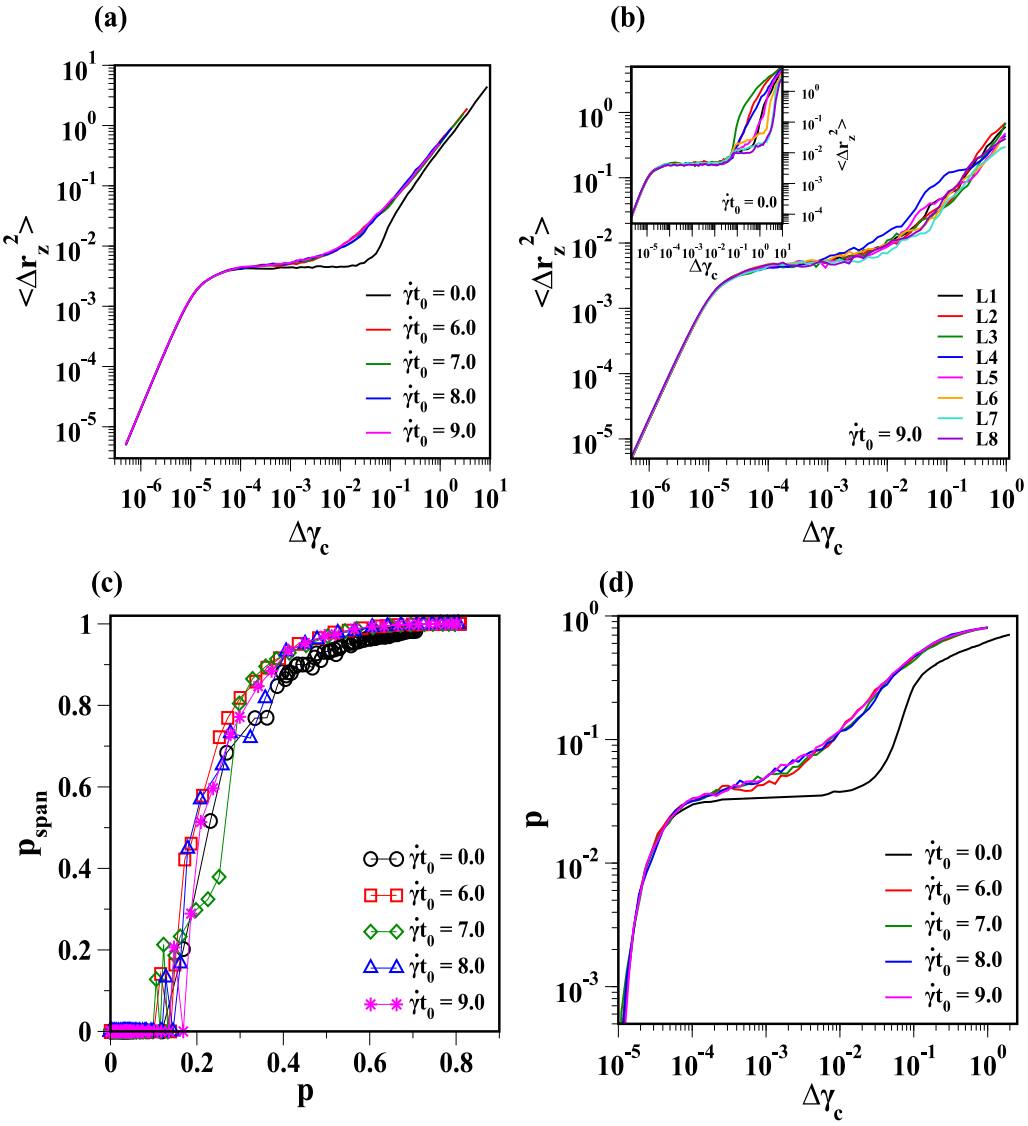

FIG. 6. Percolation transition in the steady-state regime for the $20 \times 20 \times 80$ system. (a) shows evolution of MSD with strain interval $\Delta\gamma_c$, for strain origins $\dot{\gamma}t_0 = 0.0, 6.0, 7.0, 8.0$, and 9.0, after shear is imposed. (b) Layerwise MSD. Simulation box is divided into eight layers and average MSD for each layer is plotted for a strain origin of $\dot{\gamma}t_0 = 9.0$. Inset shows the same layerwise MSD for time origin taken at the start of the shear, i.e., $\dot{\gamma}t_0 = 0.0$. (c) Percolation transition with respect to the time origins mentioned in (a). (d) Variation of p with $\Delta\gamma_c$.

in Fig. 4(c), using a 2D projection of the MSD map for the system size of 50^3. However, in this case, there are increased fluctuations at the band interface compared to the elongated geometry, wherein fluctuations are suppressed due to finite-size effects. Nevertheless, for such a cubic system, we are able to compute the spatial profiles of locally averaged MSDs, $\Delta^2(z)$. In Fig. 4(d), we show how the spatial profiles evolve with increasing strain. A large localized fluctuation in $\Delta^2(z)$ emerges beyond the strain threshold corresponding to the percolation transition. The width of this region of high mobility increases with time, similar to the discussion above. In fact, the measured ξ_b in the cubic system, for an applied $\dot{\gamma} = 10^{-4}$, has a temporal growth quite similar to what is observed in the elongated geometry; see solid green squares in Fig. 4(b). This indicates that the dynamical properties of the invading front of mobility, that eventually fluidizes the system, are not influenced by finite-size effects.

Further, we also note that the nature and extent of dynamical heterogeneities can differ, once the system starts evolving after the percolation transition has occurred. This is explored in Fig. 5.

We consider the case of two independent trajectories for the 50^3 system, evolving under applied $\dot{\gamma} = 10^{-4}$. In each case, the growth of mobile regions exhibits identical features leading to the percolation transition at strain values prior to the occurrence of the maximum in the stress-strain relation. In Figs. 5(b) and 5(f), we show the corresponding spanning clusters at the strain in the vicinity of p_c. Subsequently, the spatial organizations of the dynamical heterogeneities differ, as is seen in Figs. 5(c) and 5(g), for the respective cases, when the global strain has reached 0.5. In one case, we have shear bands parallel to the direction of flow [Fig. 5(c)], as discussed above, while in the other case the more mobile cells form structures perpendicular to the flow direction [Fig. 5(g)].

The latter response is characterized by a rapid avalanchelike spreading of mobility, resulting in extensive plastic activity as can be seen in the corresponding strain map [Fig. 5(h)]. This is in contrast to the localization of strain corresponding to shear bands forming parallel to the flow direction; see Fig. 5(d).

We also observe that thermal fluctuations play a significant role in determining the nature of dynamical heterogeneities, as expected. To show that, we compare the response under an applied shear of $\dot{\gamma} = 10^{-4}$, for the binary LJ mixture at two different state points: $\rho = 1.2$, $T = 0.20$ (results of which have been discussed so far) and at $\rho = 1.3$, $T = 0.10$. In the latter case, just like before, a percolation transition is observed at small strain values, with the corresponding spanning cluster shown in Fig. 5(j). Subsequently, at a strain of 0.5 [Fig. 5(k)], we see that a very localized region of mobility emerges with the formation of a shear band parallel to the flow direction, with not much activity elsewhere in the system. This spatial localization is also clearly visible in the corresponding strain map [Fig. 5(l)]. Such a response is in contrast to the earlier case [Figs. 5(c) and 5(d)] where far more local spots of large mobilities and consequent plastic activity are seen, in regions outside the shear band. This difference in response is due to the fact that the system at $\rho = 1.3$, $T = 0.10$ is comparably in a deeper glassy state than when at $\rho = 1.2$, $T = 0.20$, with the respective mode coupling glass transition temperatures being 0.65 and 0.435. As one travels further away from the mode coupling transition temperature, there is a decrease in local structural rearrangements induced by the interplay between thermal fluctuations and the externally applied shear, leading to more localized dynamical heterogeneities.

D. Percolation during steady flow

So far, we have discussed the dynamical response during the onset of flow in a glass from a quiescent state. We now compare these observations with the scenario during steady flow, where dynamical heterogeneities have also been observed and studied (e.g., [17,19,24]). In Fig. 6(a), we see that the transient superdiffusive regime in the average nonaffine MSD, observed during onset, is absent in the steady state [3]. Furthermore, if we spatially resolve the average MSD in layers parallel to the flow direction, we observe a clear contrast. The dynamics is spatially heterogeneous during the onset of flow, which homogenizes to a great extent in the steady state; see Fig. 6(b). Nevertheless, if we do the identification of mobile cells and their clustering (as done earlier during the onset of flow), we observe percolation transitions with respect to arbitrary strain values located in the steady-state regime [Fig. 6(c)]. The strain interval, $\Delta\gamma_c$, in which these transitions occur, is $\Delta\gamma_c \approx 0.02$ and thus about a factor of 4 smaller than the critical strain of the initial transition. Note that unlike the case of the onset of flow where the DP transition was occurring from a quiescent to a flowing state, the transitions in the steady state are between any two states of a flowing system, separated by a strain window $\Delta\gamma_c$. Then, subsequent to the percolation transitions, there is a gradual growth in the fraction of mobile cells with time [Fig. 6(d)], in contrast to the sharper jump observed during the onset of flow.

IV. CONCLUSIONS

In this work, we have explored how a model glass, subjected to a constant strain rate, evolves from a quiescent state to plastic flow. We have shown that this process is initiated by a critical phenomenon, viz., a directed percolation transition. Under shear, hot spots form in the amorphous solid, i.e., local regions in the system where particles have undergone large nonaffine displacements. These are local structural changes transforming the initial quiescent glassy state which thus cannot be regained via thermal fluctuations. Unlike liquids, this is an essential feature of the glassy state, where a strong nonlinear response to the external shear overrides thermal fluctuations. Under continuing deformation, such hot spots spatially spread with increasing strain and at a critical strain percolate. Our finite-size scaling analysis shows that this process is consistent with the DP conjecture [42,43]. Within this conjecture, a system transforms from a fluctuating state into an absorbing state, assuming that the system has no quenched disorder, as is the case in our system. In our case, the dominance of the external shear leads to the system getting irreversibly trapped into an absorbed state of the percolating cluster of hot spots.

The subsequent growth of the active regions after the DP transition depends strongly on the applied shear rate. At larger shear rates, we observe a quick proliferation of mobile spots leading to a fluidization. On the other hand, at smaller shear rates, the mobile spots spatially organize to form shear-banded structures parallel to the shear direction. In such cases, fluidization occurs by the slow diffusion of the mobile front in the shear-gradient direction, leading to sustenance of shear bands with long time scales for such small shear rates. However, for such shear rates, we also observe different flow heterogeneities, with the most mobile region structured transverse to the shear direction. In this case, there is nearly an avalanchelike process which leads to extensive fluidization of the system. Thus, in the vicinity of yield stress, there occurs a hierarchy of dynamical heterogeneities, starting from percolating structures of large mobilities occurring at a small strain, to the formation of localized structures of larger mobilities at a later strain, before the system eventually attains homogeneous flow.

It is natural that in the steady state, percolation transitions also occur, since proliferation of plastic events, i.e., regions of relatively large mobility, are always necessary for steady flow to be sustained. However, observation of this requires a sufficiently low shear rate such that the fluidized system exhibits the caging of particles over sufficient time scales. Then, the shear couples to hot spots of high mobility, as happens initially after the switch-on of the shear field from the quiescent state. In contrast to the initial percolation transition that marks the onset of plastic flow, the transitions in the steady state occur constantly over small strain intervals, thus maintaining stationary plastic flow with a homogeneous flow pattern. It remains to be investigated how these steady-state percolation transitions are related to the avalanching of plastic events, as observed in steady-state flow under athermal conditions [58–60], imprints of which have also been reported for thermal systems [61,62].

Here, our focus has been on characterizing the yielding response of thermal glasses, which are simple yield stress

fluids. There are other such soft solids, e.g., gels, for which structures are different than thermal glasses and the response could be more complex (e.g., [36–39,57]). Thus, future work needs to explore whether the yielding scenario outlined in our work is also visible in such materials.

ACKNOWLEDGMENTS

We acknowledge financial support by the Deutsche Forschungsgemeinschaft in the framework of the priority program SPP 1594 (Grant No. HO 2231/8-2).

[1] D. Rodney, A. Tanguy, and D. Vandembroucq, Modeling the mechanics of amorphous solids at different length scale and time scale, Model. Simul. Mater. Sci. Eng. **19**, 083001 (2011).

[2] J.-L. Barrat and A. Lemaitre, *Dynamical Heterogeneities in Glasses, Colloids, and Granular Materials*, edited by L. Berthier, G. Biroli, J.-P. Bouchaud, L. Cipelletti, and W. van Saarloos (Oxford University Press, Oxford, 2011), Chap. 8.

[3] J. Zausch, J. Horbach, M. Laurati, S. U. Egelhaaf, J. M. Brader, T. Voigtmann, and M. Fuchs, From equilibrium to steady state: The transient dynamics of colloidal liquids under shear, J. Phys.: Condens. Matter **20**, 404210 (2008).

[4] M. L. Falk and C. E. Maloney, Simulating the mechanical response of amorphous solids using atomistic methods, Eur. Phys. J. B **75**, 405 (2010).

[5] E. D. Knowlton, D. J. Pine, and L. Cipelletti, A microscopic view of the yielding transition in concentrated emulsions, Soft Matter **10**, 6931 (2014).

[6] F. Varnik, L. Bocquet, and J.-L. Barrat, A study of the static yield stress in a binary Lennard-Jones glass, J. Chem. Phys. **120**, 2788 (2004).

[7] R. L. Moorcroft, M. E. Cates, and S. M. Fielding, Age-Dependent Transient Shear Banding in Soft Glasses, Phys. Rev. Lett. **106**, 055502 (2011).

[8] A. Tanguy, F. Leonforte, and J.-L. Barrat, Plastic response of a 2D Lennard-Jones amorphous solid: Detailed analysis of the local rearrangements at very slow strain rate, Euro. Phys. J. E **20**, 355 (2006).

[9] C. A. Schuh, T. C. Hufnagel, and U. Ramamurty, Mechanical behavior of amorphous alloys, Acta Mater. **55**, 4067 (2007).

[10] P. C. F. Møller, S. Rodts, M. A. J. Michels, and D. Bonn, Shear banding and yield stress in soft glassy materials, Phys. Rev. E **77**, 041507 (2008).

[11] A. L. Greer, Y. Q. Cheng, and E. Ma, Shear bands in metallic glasses, Mater. Sci. Eng. R **74**, 71 (2013).

[12] T. Divoux, M. A. Fardin, S. Manneville, and S. Lerouge, Shear Banding of Complex Fluids, Ann. Rev. Fluid. Mech. **48**, 81 (2016).

[13] P. Coussot and G. Ovarlez, Physical origin of shear-banding in jammed systems, Eur. Phys. J. E **33**, 183 (2010).

[14] S. M. Fielding, Shear banding in soft glassy materials, Rep. Prog. Phys. **77**, 102601 (2014).

[15] T. Divoux, D. Tamarii, C. Barentin, and S. Manneville, Transient Shear Banding in a Simple Yield Stress Fluid, Phys. Rev. Lett. **104**, 208301 (2010).

[16] V. Chikkadi, G. Wegdam, D. Bonn, B. Nienhuis, and P. Schall, Long-Range Strain Correlations in Sheared Colloidal Glasses, Phys. Rev. Lett. **107**, 198303 (2011).

[17] R. Besseling, L. Isa, P. Ballesta, G. Petekidis, M. E. Cates, and W. C. K. Poon, Shear Banding and Flow-Concentration Coupling in Colloidal Glasses, Phys. Rev. Lett. **105**, 268301 (2010).

[18] J. Bokeloh, S. V. Divinski, G. Reglitz, and G. Wilde, Tracer Measurements of Atomic Diffusion inside Shear Bands of a Bulk Metallic Glass, Phys. Rev. Lett. **107**, 235503 (2011).

[19] F. Varnik, L. Bocquet, J.-L. Barrat, and L. Berthier, Shear Localization in a Model Glass, Phys. Rev. Lett. **90**, 095702 (2003).

[20] P. Chaudhuri and J. Horbach, Onset of flow in a confined colloidal glass under an imposed shear stress, Phys. Rev. E **88**, 040301(R) (2013).

[21] Y. Shi and M. L. Falk, Atomic-scale simulations of strain localization in three-dimensional model amorphous solids, Phys. Rev. B **73**, 214201 (2006).

[22] N. B. Bailey, J. Schiotz, and K. W. Jacobsen, Atomistic simulation study of the shear-band deformation mechanism in Mg-Cu metallic glasses, Phys. Rev. B **73**, 064108 (2006).

[23] M. Tsamados, A. Tanguy, C. Goldenberg, and J.-L. Barrat, Local elasticity map and plasticity in a model Lennard-Jones glass, Phys. Rev. E **80**, 026112 (2009).

[24] M. Tsamados, Plasticity and dynamical heterogeneity in driven glassy materials, Euro. Phys. J. E **32**, 165 (2010).

[25] C. Fusco, T. Albaret, and A. Tanguy, Rheological properties vs. local dynamics in model disordered materials at low temperature, Eur. Phys. J. E **37**, 43 (2014).

[26] P. Chaudhuri, L. Berthier, and L. Bocquet, Inhomogeneous shear flows in soft jammed materials with tunable attractive forces, Phys. Rev. E **85**, 021503 (2012).

[27] R. Dasgupta, H. G. E. Hentschel, and I. Procaccia, Microscopic Mechanism of Shear Bands in Amorphous Solids, Phys. Rev. Lett. **109**, 255502 (2012).

[28] E. Irani, P. Chaudhuri, and C. Heussinger, Impact of Attractive Interactions on the Rheology of Dense Athermal Particles, Phys. Rev. Lett. **112**, 188303 (2014).

[29] D. Vandembroucq and S. Roux, Mechanical noise dependent aging and shear banding behavior of a mesoscopic model of amorphous plasticity, Phys. Rev. B **84**, 134210 (2011).

[30] K. Martens, L. Bocquet, and J.-L. Barrat, Connecting Diffusion and Dynamical Heterogeneities in Actively Deformed Amorphous Systems, Phys. Rev. Lett. **106**, 156001 (2011).

[31] K. Martens, L. Bocquet, and J.-L. Barrat, Spontaneous formation of permanent shear bands in a mesoscopic model of flowing disordered matter, Soft Matter **8**, 4197 (2012).

[32] R. L. Moorcroft and S. M. Fielding, Criteria for Shear Banding in Time-Dependent Flows of Complex Fluids, Phys. Rev. Lett. **110**, 086001 (2013).

[33] A. Amon, A. Bruand, J. Crassous, and J. Clément, Hot Spots in an Athermal System, Phys. Rev. Lett. **108**, 135502 (2012).

[34] T. Sentjabrskaja, P. Chaudhuri, M. Hermes, W. C. K. Poon, J. Horbach, S. U. Egelhaaf, and M. Laurati, Microscopic dynamics during creep in colloidal glasses, Sci. Rep. **5**, 11884 (2015).

[35] P. Moller, A. Fall, V. Chikkadi, D. Derks, and D. Bonn, An attempt to categorize yield stress fluid behaviour, Phil. Trans. R. Soc. A **367**, 5139 (2009).

[36] T. Gibaud, C. Barentin, and S. Manneville, Influence of Boundary Conditions on Yielding in a Soft Glassy Material, Phys. Rev. Lett. **101**, 258302 (2008).

[37] J. D. Martin and Y. T. Hu, Transient and steady-state shear banding in aging soft glassy materials, Soft Matter **8**, 6940 (2012).

[38] A. Kurokawa, V. Vidal, K. Kurita, T. Divoux, and S. Manneville, Avalanche-like fluidization of a non-Brownian particle gel, Soft Matter **11**, 9026 (2015).

[39] T. Mohoric, J. Dobnikar, and J. Horbach, Two-dimensional magnetic colloids under shear, Soft Matter **12**, 3142 (2016).

[40] F. Leonforte, A. Tanguy, J. P. Wittmer, and J.-L. Barrat, Inhomogeneous Elastic Response of Silica Glass, Phys. Rev. Lett. **97**, 055501 (2006).

[41] C. L. Rountree, D. Vandembroucq, M. Talamali, E. Bouchaud, and S. Roux, Plasticity-Induced Structural Anisotropy of Silica Glass, Phys. Rev. Lett. **102**, 195501 (2009).

[42] H. K. Janssen, On the nonequilibrium phase transition in reaction-diffusion systems with an adsorbing stationary state, Z. Phys. B **42**, 151 (1981).

[43] P. Grassberger, On phase transitions in Schlögl's second model, Z. Phys. B **47**, 365 (1982).

[44] H. Hinrichsen, Non-equilibrium critical phenomena and phase transitions into absorbing states, Adv. Phys. **49**, 815 (2000).

[45] P. Rupp, R. Richter, and I. Rehberg, Critical exponents of directed percolation measured in spatiotemporal intermittency, Phys. Rev. E **67**, 036209 (2003).

[46] A. Franceschini, E. Filippidi, E. Guazzelli, and D. J. Pine, Transverse Alignment of Fibers in a Periodically Sheared Suspension: An Absorbing Phase Transition with a Slowly Varying Control Parameter, Phys. Rev. Lett. **107**, 250603 (2011).

[47] W. Kob and H. C. Andersen, Scaling Behavior in the β-Relaxation Regime of a Supercooled Lennard-Jones Mixture, Phys. Rev. Lett. **73**, 1376 (1994).

[48] S. Plimpton, Fast Parallel Algorithms for Short-Range Molecular Dynamics, J. Comp. Phys. **117**, 1 (1995).

[49] T. Soddemann, B. Dünweg, and K. Kremer, Dissipative particle dynamics: A useful thermostat for equilibrium and nonequilibrium molecular dynamics simulations, Phys. Rev. E **68**, 046702 (2003).

[50] A. W. Lees and S. F. Edwards, The computer study of transport processes under extreme conditions, J. Phys. C **5**, 1921 (1972).

[51] K. N. Nordstrom, E. Verneuil, P. E. Arratia, A. Basu, Z. Zhang, A. G. Yodh, J. P. Gollub, and D. J. Durian, Microfluidic Rheology of Soft Colloids above and below Jamming, Phys. Rev. Lett. **105**, 175701 (2010).

[52] P. Chaudhuri and J. Horbach, Poiseuille flow of soft glasses in narrow channels: From quiescence to steady state, Phys. Rev. E **90**, 040301(R) (2014).

[53] D. Stauffer and A. Aharony, *Introduction to Percolation Theory*, 2nd ed. (Taylor & Francis, London, 2003).

[54] J. Wang, Z. Zhou, Q. Liu, T. M. Garoni, and Y. Deng, High-precision Monte Carlo study of directed percolation in $(d+1)$ dimensions, Phys. Rev. E **88**, 042102 (2013).

[55] M. A. Munõz, R. Dickman, A. Vespignani, and S. Zapperi, Avalanche and spreading exponents in systems with absorbing states, Phys. Rev. E **59**, 6175 (1999).

[56] M. C. T. P. Carvalho and J. A. M. S. Duarte, Directed-Site Percolation Clusters: The Scaling Function in Dimensions Two to Six, Z. Phys. B **70**, 203 (1988).

[57] T. Divoux, D. Tamarii, C. Barentin, S. Teitel, and S. Manneville, Yielding dynamics of a Herschel-Bulkley fluid: a critical-like fluidization behaviour, Soft Matter **8**, 4151 (2012).

[58] A. Lemaitre and C. Caroli, Rate-Dependent Avalanche Size in Athermally Sheared Amorphous Solids, Phys. Rev. Lett. **103**, 065501 (2009).

[59] N. P. Bailey, J. Schiøtz, A. Lemaître, and K. W. Jacobsen, Avalanche Size Scaling in Sheared Three-Dimensional Amorphous Solid, Phys. Rev. Lett. **98**, 095501 (2007).

[60] S. Karmakar, E. Lerner, and I. Procaccia, Statistical physics of the yielding transition in amorphous solids, Phys. Rev. E **82**, 055103(R) (2010).

[61] H. G. E. Hentschel, S. Karmakar, E. Lerner, and I. Procaccia, Size of Plastic Events in Strained Amorphous Solids at Finite Temperatures, Phys. Rev. Lett. **104**, 025501 (2010).

[62] J. Chattoraj, C. Caroli, and A. Lemaitre, Universal Additive Effect of Temperature on the Rheology of Amorphous Solids, Phys. Rev. Lett. **105**, 266001 (2010).